Journal of Organometallic Chemistry 899 (2019) 120892

Contents lists available at ScienceDirect

Journal of Organometallic Chemistry

journal homepage: www.elsevier.com/locate/jorganchem

Hydrogenation of carbon dioxide to formate by α-diimine Ru^{II}, Rh^{III}, Ir^{III} complexes as catalyst precursors

Nyasha Makuve [a], Gift Mehlana [b], Richard Tia [c], James Darkwa [a], Banothile C.E. Makhubela [a, *]

[a] Department of Chemistry, University of Johannesburg, Kingsway Campus, P.O. Box 524, Auckland Park, 2006, Johannesburg, South Africa
[b] Department of Chemical Technology, Midlands State University, Private Bag 9055 Senga Road, Gweru, Zimbabwe
[c] Department of Chemistry, Kwame Nkrumah University of Science and Technology, Kumasi, Ghana

ARTICLE INFO

Article history:
Received 16 June 2019
Received in revised form
26 July 2019
Accepted 12 August 2019
Available online 15 August 2019

Keywords:
CO_2 hydrogenation
Homogeneous catalysis
α-diimine complexes
Mechanistic studies
DFT calculations

ABSTRACT

The conversion of CO_2 into valuable chemicals has been of major interest because it is cheap and readily available. The concept of reducing CO_2 pollution *via* its utilization into valuable products has inspired us to synthesise novel 4,4'-((1Z)-butane-2,3-diylidenebis(azanylylidene))dibenzoic acid (**L**) metal complexes {[(L)Ru^{II}] (**C1**), [(L)Rh^{III}] (**C2**), [(L]Ir^{III} (**C3**)} complexes for catalytic hydrogenation of CO_2. The α-diimine metal complexes (**C1**–**C3**) were characterised using several analytical techniques, including: NMR spectroscopy and single crystal X-ray crystallography. In a mixture of THF/H_2O and a base, all three catalyst precursors were able to hydrogenate CO_2 cleanly to formate as a product. However, the best combination of catalyst precursor and a base was **C1** and DBU that selectively produced formate at a moderate temperature of 120 °C and at 60 bar. The best productivity under these conditions is TOF of 35 h^{-1} within 2 h and a TON of 322. This work is significant because it provides a one-step synthesis for formate from CO_2 using α-diimine-based complexes which can be synthesised in a one-step reaction. The density functional theory calculations on **C1** supports that Ru–H is the active species in the process of CO_2 hydrogenation to formate with the insertion of the CO_2 to Ru–H being the rate determining step.

1. Introduction

The catalytic conversion of CO_2 to formic acid or formate has attracted much attention due to the useful properties of formic acid in the chemical and pharmaceutical industries. Hydrogenation of CO_2 to formic acid catalysed by half-sandwich transition metal complexes of Ru, Rh, Ir, Mn and Co have been studied both practically and theoretically using DFT studies [1,2]. Iridium-based half sandwich complexes are more catalytic active towards the formation of formic acid [3]. Kanega and co-workers have reported the direction hydrogenation of CO_2 to formate with half sandwich Ir-based complexes containing picolinamide and picolinic acid derivatives as pre-catalysts. Under mild conditions of 0.1 MPa and 25 °C in water pre-catalyst containing 4-hydroxy -*N*-methylpicolinamidate produced 0.64 M formate with a turn over number (TON) of 14 700 and turn over frequency (TOF) of 167 h^{-1} [4]. The excellent catalytic performance by the Ir-4-hydroxy -*N*-methylpicolinamidate complex was attributed to the strong electron donation by the phenolic O^- functionality and anionic amide moiety.

A minireview by Himeda on the hydrogenation of CO_2 to formic acid catalysed by half sandwich complexes of Ru, Rh and Ir containing 4,7-dihydroxy-1,10-phenathroline and 4,4-dihydroxy-2,2-bipyridine ligands attributes the high catalytic performance of these groups 8 and 9 metal complexes to the water solubility of the catalysts, their electron effect and the polarity of the oxyanion generated from phenol hydroxyl group when these metal complexes are dissolved in water [5]. Indeed hydrogenation of CO_2 to formic acid has not only been observed in water but also in alcoholic solvents and mixtures of solvents [6]. The addition of a base in the hydrogenation process of CO_2 to formate has been reported to change the reaction rate. The organic base 1,8-diazabicyclo[5.4.0] undec-7-ene (DBU) base appears to be the best performing with TON of 95 000 reported in the presence of trimethylphosphino

* Corresponding author.
E-mail address: bmakhubela@uj.ac.za (B.C.E. Makhubela).

https://doi.org/10.1016/j.jorganchem.2019.120892
0022-328X/

ruthenium complexes as pre-catalysts [7].

Recently there has been a growing interest in the hydrogenation of CO_2 to formate with bipyridine half sandwich complexes. The studies have been focusing on the effect of strong electron donating phenolic functionalities on the co-ligands and the water-soluble catalyst for the hydrogenation of CO_2 to formic acid [8]. Of interest, none of the publications focus on α-diimine half-sandwich complexes with carboxylic acid moieties for the same hydrogenation of CO_2 to formate.

It is clear from the above narrative that to have an effective CO_2 hydrogenation catalyst, you need a pre-catalyst and a base that are both soluble in the solvent in which you run the hydrogenation reaction. In this contribution, novel α-diimine-based complexes containing carboxylic acid moieties for the catalytic hydrogenation of CO_2 will be investigated with mechanistic studies evaluated using density functional theory calculation. In this study we synthesised novel cationic N^N Ru^{II}, Rh^{III} and Ir^{III} complexes (**C1**–**C3**) that are soluble in solvent mixtures and evaluate their ability to hydrogenate of CO_2 to formate. The best catalyst for CO_2 hydrogenation reaction to formate Ru complex (**C1**) as pre-catalyst in the presence THF/H_2O mixture, DBU and a ratio of 1:4 CO_2:H_2 with total pressure of 60 bar.

2. Experimental

2.1. Materials and methods

All air and moisture sensitive compounds were manipulated using standard Schlenk and vacuum line techniques under an argon atmosphere. Argon HP/zero -grade, carbon dioxide gas HP/zero -grade and hydrogen gas HP/zero-grade (>99%) were purchased from Afrox Gases (South Africa). Potassium hydroxide, absolute ethanol, acetonitrile, toluene, methanol, chloroform, tetrahydrofuran (THF), dichloromethane (DCM) and dimethyl sulfoxide (DMSO) were purchased from Rochelle Chemicals (South Africa). 4-aminobenzoic acid (Sigma-Aldrich, >99%), 2,3 Butanedione (Sigma-Aldrich, 97%), chloroform-d, dimethyl sulfoxide–d_6 (DMSO-d_6), N,*N*-dimethylformamide anhydrous (DMF) (Sigma-Aldrich, 99.8%), glyme (Sigma-Aldrich, >99%), 1,8-diazabicyclo[5.4.0]undec-7-ene (DBU) (Sigma-Aldrich, 98%), pentamethylcyclopentadiene, $IrCl_3.3H_2O$, $RhCl_3.3H_2O$ and $RuCl_3.3H_2O$ were purchased from Sigma-Aldrich. The metal precursors of $[Cp^*IrCl_2]_2$, $[Cp^*RhCl_2]_2$ and Ru(p-cymene)Cl_2] were synthesised according to literature methods [9,10]. ^1H and ^{13}C NMR spectra were recorded on a Bruker Ultrashield 400 MHz (^1H: 400 MHz; ^{13}C:100 MHz) spectrometer. All chemical shift values are reported relative to the internal standard tetramethylsilane (δ 0:00) and in ppm. FT-IR spectra were recorded on a PerkinElmer FT-IR Spectrum BX Spectrometer. Elemental analysis was carried out using the Thermo Scientific Flash 2000 CHNSO analyser. ES1-MS was determined at Stellenbosch University Central Analytical Services on a Waters Synapt G2 mass spectrometer. All CO_2 hydrogenation reactions were performed in high pressure vessels, to a parallel high-pressure autoclave with inbuilt stirring, heating and cooling system. ^1H and $^{13}C\{^1H\}$ NMR chemical shifts for the hydrogenation products were determined relative to the internal standard DMF.

Precaution: Proper safety measures must be observed as well as use of personal protective equipment whilst handling H_2 and CO_2 gases (molecular) at experimental conditions.

2.2. Synthesis and characterisation of ligand and complexes

2.2.1. 4,4'-((1Z)-butane-2,3-diylidenebis(azanylylidene))dibenzoic acid (*L*)

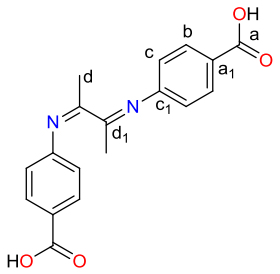

2,3-Butanedione (150.01 mg; 1.745 mmol) was dissolved in 20 mL MeOH and the solution stirred for 4 min before adding 4-aminobenzoic acid (480.00 mg; 3.485 mmol) dissolved in 30 mL MeOH. The reaction mixture was then refluxed for 48 h to afford a bright yellow solution. After removal of the solvent on a rotary evaporation to give a yellow solid, the product was dried in *vacuo* for 4 h. Yield: 430.02 mg, 76%. Melting point: decomposes without melting (onset at 228 °C). ^1H NMR (DMSO-d_6) (ppm): δ 12.78 (br, 2H, H_a), 7.96 (d, 4H, $^3J_{H\text{-}H} = 8.0$ Hz, H_b), δ 6.91 (d, 4H, $^3J_{H\text{-}H} = 8.0$ Hz, H_c), δ 2.05 (s, 6H, H_d)). $^{13}C\{^1H\}$ NMR (DMSO-d_6) (ppm): δ 167.64 (Ca), δ 166.99 (Cd_1), δ 154.44 (Ca_1), δ 130.59 (Cc_1), δ 126.20 (C_b), δ 118.51 (C_c), δ 15.36 (C_d). FT-IR (cm^{-1}): υ(C=O) 1681, υ(C=N) 1601. Solubility: insoluble in DCM, EtOH, MeOH, THF; soluble in DMSO, DMF and partially soluble in water. Elemental analysis: Found: C 66.85, H 4.98, N 8.65%. Calculated: C 66.66, H 4.97, N 8.64%.

2.2.2. [Ru(p-cymene)Cl(*L*)]Cl (*C1*)

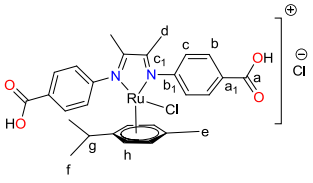

Compound **L** (240.00 mg; 0.73 mmol) was dissolved in EtOH (15 mL) and stirred for 10 min before adding a solution of [$RuCl_2$ (p-cymene)]$_2$ (220.03 mg; 0.36 mmol) in 5 mL of ethanol. The reaction mixture was stirred at room temperature for 24 h to give a brown precipitate. The precipitate was recovered by vacuum filtration, washed off with ethanol and dried in *vacuo* for 6 h to give the product as a pure brown solid. **Yield**: 440.04 mg, 90%. Melting point: decomposes without melting (onset at 228 °C). ^1H NMR (DMSO-d_6) (ppm)): δ 12.78 (s, 2H, H_a), 7.96 (d, 4H, $^3J_{H\text{-}H} = 8.4$ Hz, H_b), 6.92 (d, 2H, $^3J_{H\text{-}H} = 8.4$ Hz, H_c), 5.78 (dd, 4H, $^3J_{H\text{-}H} = 6$ Hz, $H_{f1,f2}$), 2.82 (m, 1H, H_g), 2.05 (d, 9H, $^3J_{H\text{-}H} = 4.4$ Hz, $H_{d,e}$), 1.18 (d, 6 H, $^3J_{H\text{-}H} = 6.8$ Hz, H_h). $^{13}C\{^1H\}$ NMR (DMSO-d_6) (ppm)): δ 166.78 (Ca), 152.43 (Cc_1), 130.50 (Cb_1), 116.12 (Cb), 112.82 (Ca_1), 105.64 (Cc), 99.36 (Cg), 85.65 (Ch), 84.79 (Ch_1), 29.26 (Cf), 20.78 (Ce), 17.15 (Cd). FT-IR (cm^{-1}): υ(C=O) 1678, υ(C=N) 1599. Elemental analysis: Found: C 54.17, H 5.33, N 4.50%. Calculated: C 54.46, H 5.64, N 4.23%. HR-ESI-MS (*m/z*): $[M + H]^+ = 627.1658$. Solubility: insoluble in DCM, water, toluene; soluble in THF, acetonitrile, DMSO, DMF, partially solubility in MeOH, partially solubility in EtOH and partially soluble in Acetone. Compounds **C2** and **C3** were prepared in a similar manner as described for **C1** using the appropriate

starting materials indicated for each compound.

2.2.3. [Ir(Cp*)Cl**L**]Cl (**C2**)

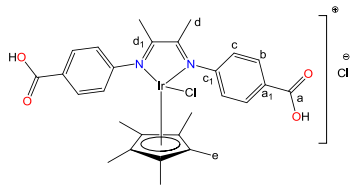

Compound **C2** was prepared from **L** (250.03 mg; 0.76 mmol) in 15 mL EtOH and $[Ir(\eta^5\text{-}C_5Me_5)Cl_2]_2$ (300.00 mg; 0.38 mmol) in 5 mL EtOH. Yield: 240.01 mg, 96%. Melting point: 250–252 °C. ^{1}H NMR (DMSO-d_6) (ppm)): δ 12.78 (br, 2H, H_a), 7.95 (d, 2H, $^3J_{H\text{-}H} = 8.2$ Hz, H_c), 6.91 (d, 4H, $^3J_{H\text{-}H} = 8.2$ Hz, H_b), 2.05 (s, 6H, H_d), 1.61 (s, 15 H, H_e). FT-IR (cm^{-1}): υ(C═O) 1679, υ(C═N) 1600. $^{13}C\{^1H\}$ NMR (DMSO-d_6) (ppm)): δ 167.69 (Ca), 167.04 (Cd_1), 154.49 (Cc_1), 130.64 (Cb), 126.22 (Ca_1), 118.56 (Cc), 92.10 (Cp* aromatic ring), 15.43 (Cd), 8.26 (Ce). HR-ESI-MS (*m/z*): $[M + Cl]^- = 771.0347$. Solubility: insoluble in DCM, MeOH, toluene; soluble in DMF, DMSO, partially soluble in EtOH and partially soluble in water. Elemental analysis: Found: C 47.10, H 4.63, N 3.75%. Calculated: C 47.21, H 4.65, N 3.80%.

2.2.4. [Rh(Cp*)Cl**L**]Cl (**C3**)

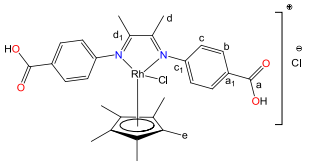

Compound **C3** was prepared from **L** (240.02 mg; 0.74 mmol) in 15 mL EtOH and $[Rh(\eta^5\text{-}C_5Me_5)Cl_2]_2$ (300.01 mg; 0.38 mmol) in 5 mL EtOH. Yield: 435.88 mg, 95%. Melting point: 251–253 °C. ^{1}H NMR (DMSO-d_6) (ppm): δ 12.79 (br, 2H, H_a), 7.95 (d, 4H, $^3J_{H\text{-}H} = 8.3$ Hz, H_b), 6.91 (d, 4H, $^3J_{H\text{-}H} = 8.3$ Hz, H_c), 2.05 (s, 6H, H_d), 1.61 (s, 15 H, H_e). $^{13}C\{^1H\}$ NMR (DMSO-d_6) (ppm)): δ 167.69 (Ca), 167.04 (Cd_1), δ 154.49 (Cc_1), 130.64 (Cb), 126.22 (Ca_1), 118.56 (Cc), 92.10 (Cp* aromatic ring), 15.43 (Cd), 8.26 (Ce). Solubility: insoluble in DCM, MeOH, toluene; soluble in DMF, DMSO, partially soluble in EtOH and partially soluble in water. Elemental analysis: Found: C 53.42, H 5.10, N 4.14%. Calculated: C 53.72, H 5.29, N 4.32%. FT-IR (cm^{-1}): υ(C═O) 1678, υ(C═N) 1599. HR-ESI-MS (*m/z*): $[M + H]^+ = 613.1390$.

2.3. General procedure for the hydrogenation of CO_2

In a typical experiment a pre-catalyst (7 μmol), DBU (4.20 mmol), THF (5 mL) and H_2O (1 mL) were mixed in 4 × 50 mL stainless reactor vessels. Each reactor vessel was flushed three cycles with nitrogen gas, followed by addition of CO_2 gas and H_2 gas (1:2, CO_2/H_2 bar) to give a total pressure of 60 bar. The reactor vessels were transferred to a preheated EYELA parallel reactor block at 120 °C and at a stirring speed of 1000 rpm (a magnetic stir bar was used to stir) and reaction run for 24 h. The reactor then was cooled to room temperature followed by carefully venting of the reactor. The reaction mixture was analyzed by ^{1}H NMR and ^{13}C NMR spectroscopy using DMF as an internal standard. In a separate reaction, the homogeneity of the catalytic reaction was tested by the mercury poisoning test.

2.4. Computational studies of the catalytic hydrogenation of CO_2

To investigate the mechanism of the hydrogenation reactions, that catalytic reaction was modelled with Spartan'14 and Gaussian'09 molecular modelling packages. Starting geometries were constructed with Spartan'14 graphical model builder. All geometries were optimized, and IR frequencies calculated to ensure that transition states have only one imaginary frequency vibrating along the reaction coordinate and all minima have no imaginary frequencies. Single point energies were calculated for H and Cl anions as there were no bonds to be optimized. All reported energies are relative Gibbs free energies. DFT MO6 calculations were carried out with Gaussian using 6-31G* basis set augmented with quasi-relativistic pseudo-potential, LANL2DZ, for the metal centre. All calculations were carried out in *vacuo* at 298 K.

3. Results and discussion

3.1. Synthesis and characterisation of **L**

The synthesis of compound **L** was performed by refluxing 2,3-butanedione and two mole equivalents of 4-aminobenzoic acid in dry methanol (Scheme 1) using reported literature methods [11,12] to give a bright yellow solid that was isolated in a high yield of 76%. Ligand **L** is not a new, nevertheless it was characterised by ^{1}H and $^{13}C\{^1H\}$ NMR spectroscopy, FT-IR spectroscopy and elemental analysis (CHN). Evidence of the successful Schiff base reaction was seen in the ^{1}H NMR spectrum (Fig. S1) with the aromatic protons observed as doublets, integrating for four protons each, at 7.96 ppm and 6.91 ppm; having *J* values of 8.00 Hz each. The *J* values of 8.00 Hz are characteristic of aromatic protons. The methyl protons were observed as a singlet at 2.05 ppm. The $^{13}C\{^1H\}$ NMR of **L** (Fig. S2) shows a singlet resonance at 166.99 ppm which is a characteristic imine carbon with no ketone carbonyl signals from the 2,3-butanedione starting material. These results are in agreement with previously reported literature results [12].

The infrared spectroscopic results further substantiate that the imine functionality is present, with the υ(C═N) absorption band at 1601 cm^{-1}. The other absorption band observed at 1681 cm^{-1} is for the carbonyl group (C═O). Elemental analysis results show that **L** is pure with the calculated results being very similar to the experimental results.

3.2. Synthesis and characterisation of C1–C3

Synthesis of complexes **C1**–**C3** was achieved by reacting ligand **L** with corresponding metal precursors as shown in Scheme 2. Other counter anions such as triflate were considered but products were air and moisture sensitive. The coordination of α-diimine nitrogen of **L** to the ruthenium-arene moiety to form complex **C1** was confirmed by ^{1}H NMR spectroscopy. The ^{1}H NMR spectra of

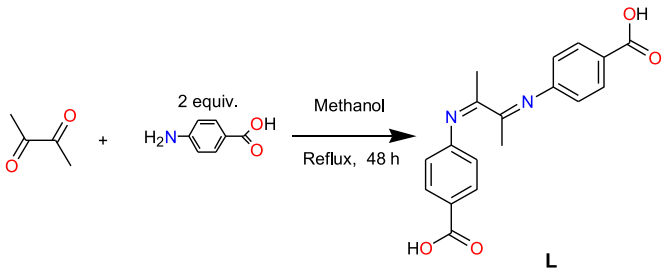

Scheme 1. Schematic illustration of synthesis of N^N ligand **L**.

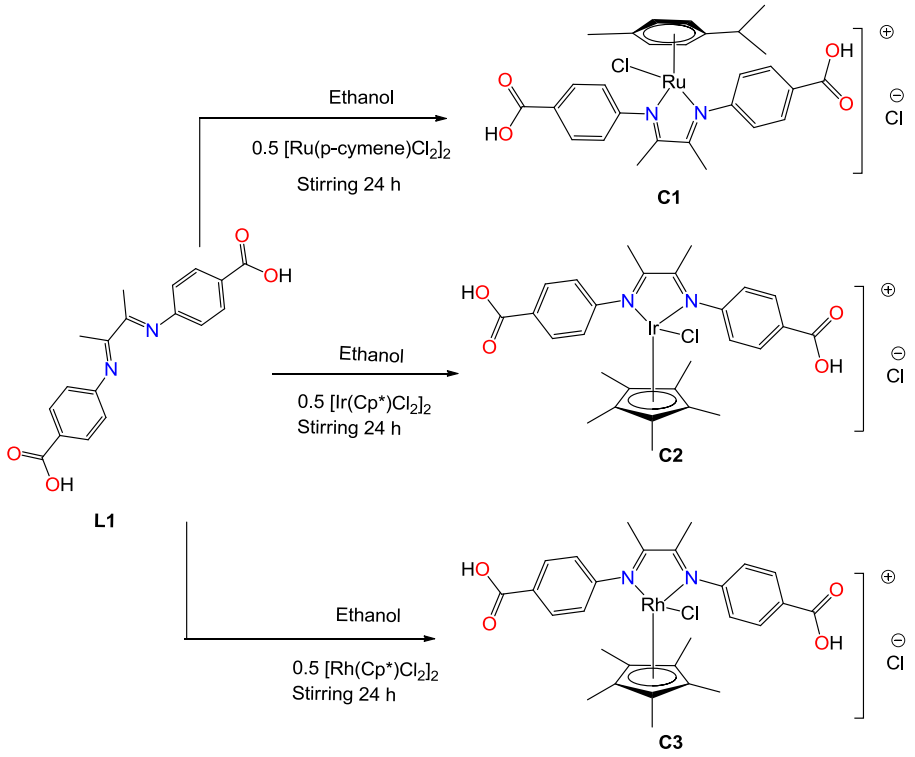

Scheme 2. Schematic illustration of the synthesis **C1**–**C3**.

complex **C1** (Fig. S3) showed characteristic signals associated with ruthenium dimer complexation relative to the free ligand L. ^{1}H NMR spectra showed a had a downfield shift of the aromatic protons from 6.91 ppm for **L** to 6.92 ppm in **C1.** Minimal chemical shifts are expected due to a greater influence of the metal coordination on the aromatic protons *ortho*-to the imine nitrogen atoms observed at 6.91 ppm in the ligand **L** than the *meta*-position protons. This shift confirms that the nitrogen atoms are coordinated to the ruthenium metal centre by displacement of a chloride. The signal for the four aromatic protons of p-cymene moiety in **C1** were observed as two doublets due to the perpendicular plane position of the p-cymene moiety to the metal. The presence of the p-cymene moiety was also evidence that the complexation was successful.

The ^{1}H NMR spectra of Ir (**C2**) (Fig. S4) and Rh (**C3**) (Fig. S5) complexes showed the $-CH_3$ protons for iridium and rhodium Cp* at 1.61 ppm for both complexes. These protons were observed in the same region due to their perpendicular plane position to the metal. The $^{13}C\{^{1}H\}$ NMR spectra of all three complexes **C1**–**C3** (Figs. S6–8) showed a downfield shift of the imine carbon from 166.99 ppm to about 167.04 ppm with all other aromatic and alkyl chain carbons being accorded for in their respective regions. Elemental analysis, FT-IR absorption band shifts for the imine functionality and high-resolution electrospray ionisation mass spectrometry further confirmed the formation of the three complexes.

Orange single crystals of complex **C3**, suitable for XRD analysis were grown by slow diffusion of n-hexane (0.5 mL) into a concentrated solution of C3 in DMF (0.2 mL) and DCM (0.1 mL) at ambient temperature. Complex **C3** crystallises in a monoclinic crystal system in the space group $P2_1/n$ (primitive two-fold screw axis) (Table S1). The two imine nitrogen atoms are coordinated to the rhodium centre forming a piano stool octahedral geometry complex around the rhodium metal centre (Fig. 1). The bond lengths along the Rh metal centre of Rh(1)–N(1)(2.097 Å), Rh(1)-N(2)(2.094 Å) and Rh(1)–Cl(1) (2,4073 Å) fall within literature reported values [13,14]. Structural analysis of the complex in PLATON

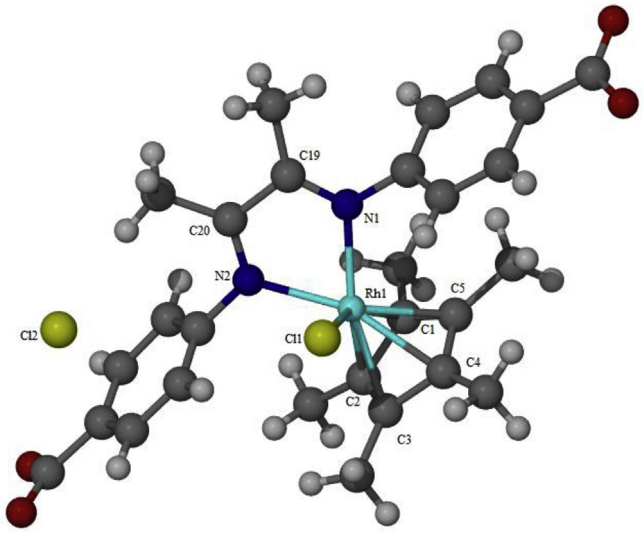

Fig. 1. Crystal structure for complex **C3** with hydrogen atoms omitted for clarity. Selected bond lengths (Å): Rh(1)–Cl(1), 2.4073(9), 87; Rh(1)–N(2), 2.097(3),; Rh(1)–N(1), 2.094(3), Rh(1)–C(1); 2.152(4), Rh(1)–C2(1), 2.171(4); Rh(1)–C(3), 2.193(3); Rh(1)–C(4), 2.157(4); Rh(1)–C(5), 2.191(4). Selected bond angles (deg.): N(2)-Rh(1)-Cl(1), 87.56(8); N(2)-Rh(1)-C(1), 163.47(13); N(2)-Rh(1)-C(1), 124.17(13); N(1)-Rh(1)-Cl(1), 86.86(9); N(1)-Rh(1)-N(2), 75.31(12); N(1)-Rh(1)-C(1), 121.16(13); C(1)-Rh(1)-Cl(1), 94.45(11); C(1)-Rh(1)-C(2), 39.38 (14); C(1)-Rh(1)-C(3), 64.81 (14); C(1)-Rh(1)-C(4), 65.16 (14); C(1)-Rh(1)-C(5), 38.33 (14).

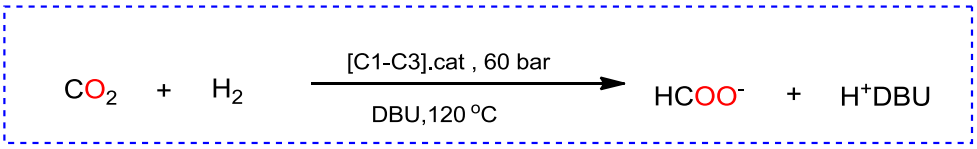

Scheme 3. Direct hydrogenation of CO_2 to formate.

Table 1
Initial hydrogenation of CO_2 with pre-catalysts **C1**–**C3**.

Entry	Cat.	Solvent	Pressure (bar)	$HCOO^-$ (mmol)	TON	TOF (h^{-1})
1	**C1**	THF/H_2O	60	1.9	270	11
2	**C2**	THF/H_2O	60	1.3	190	7.7
3	**C3**	THF/H_2O	60	0.6	86	3.6

Conditions: DBU base (4.20 mmol), CO_2 (20 bar), H_2 (40 bar), 120 °C, THF (5 mL), H_2O (1 mL), and 24 h. Cat. = pre-catalyst; cat loading (7 μmol). Products were determined by ^1H NMR and $^{13}C\{^1H\}$ NMR spectroscopy in the presence of DMF (10 μL) as an internal standard. Average error estimate: **C1** = ±0.20, **C2** = ±0.18, **C3** = ±0.19.TON = (mmol of formate/mmol of pre-catalyst). TOF = TON/reaction time.

[15,16] shows that there are no classic hydrogen bonds in compound **C3**.

3.3. Catalytic hydrogenation of CO_2 using C1–C3

The direct hydrogenation of CO_2 was explored using the synthesised complexes **C1**–**C3** as pre-catalysts as in Scheme 3.

The pre-catalysts **C1**–**C3** were first investigated as catalysts in the hydrogenation of CO_2 at 60 bar of 1:2 CO_2/H_2 using THF and H_2O as solvents and the strong organic base 1,8-Diazabicyclo[5.4.0] undec-7-ene (DBU). Results of the catalytic tests are summarized in Table 1. From these experiments (Table 1) pre-catalyst **C1** (Entry 1) was found to be the most active pre-catalyst in producing formate (1.91 mmol) as the only product under the reaction conditions. **C1**, ruthenium (II) pre-catalyst was found to be three times better than **C3** a rhodium (III) pre-catalyst which had 0.60 mmol formate and a TON of 86 (Entry 3). The ruthenium (II) pre-catalyst was the best performing and this could have been due to the basic nature of the reaction medium. In literature is has been reported that the ruthenium hydride active species is stable and very active in basic solutions during catalytic hydrogenation of CO_2 to formate [17]. The iridium (III) pre-catalyst **C2** produced 1.3 mmol of formate with a TON of 190 with was double that of **C3. C2** had a better TON value compared to some Ir (III) catalysts in literature by Wang who had a TON value of 50 (TOF 30 h^{-1}) [18] and Tanaka with TON value of 43 (TOF 1 h^{-1}) [19]. **C1** results are superior to the results reported by Man and co-workers who hydrogenated CO_2 to formate with Ru-based complexes at 120 °C for 45 h with a total pressure of 60 bar and achieved a TON value of 43 and TOF value of 1 h^{-1} [20]. Fig. S12 shows the ^1H NMR spectrum of formate ($HCOO^-$) as a singlet at 8.28 ppm and a typical formate peak in the $^{13}C\{^1H\}$ NMR spectrum (Fig. S13) at 170.01 ppm.

3.3.1. Effect of catalyst loading on hydrogenation of CO_2 with C1

In the hydrogenation of CO_2 to formate under our conditions (Fig. 2), a catalyst played a vital role because in the absence of a catalyst the reaction does not proceed thus no formate produced. Formate started to form with a minimum catalyst loading of 1 μmol giving a TON value of 320 which was the highest TON achieved under our reaction conditions. The formate concentration increase with increase in catalyst from 1 to 7 μmol which shows that the reaction is first order dependence with respect to catalyst loading. Further increase in catalyst loading from 7 to 10 μmol did not show any significant change in hydrogenation products possibly due to insignificant variation in liquid solid mass transfer.

3.3.2. Homogeneity evaluation of the hydrogenation of CO_2 with pre-catalyst *C1*

The mercury poisoning test is used to establish if a homogenous catalytic reaction is indeed truly homogeneous and not produce nanoparticle that could also catalyse a reaction. As such the mercury poisoning tests were conducted using **C1** and elemental mercury in the hydrogenation of CO_2. There was no significant drop

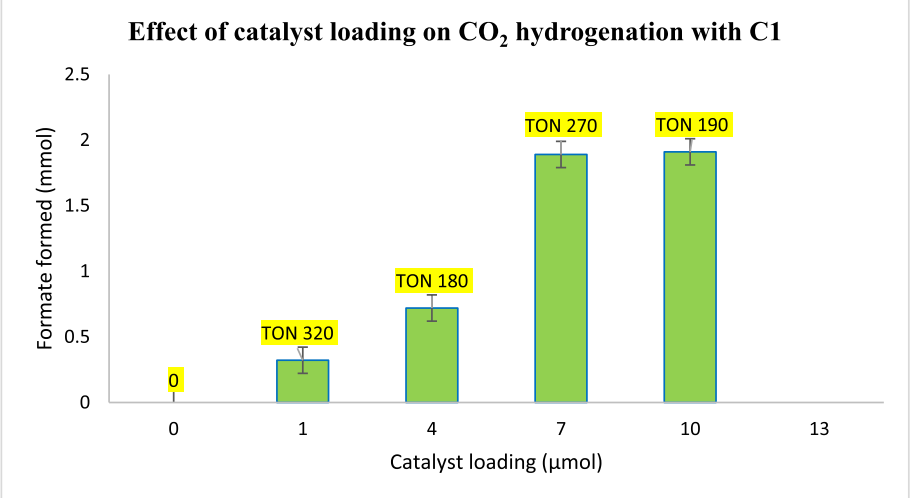

Fig. 2. Effect of catalyst loading on CO_2 hydrogenation with pre-catalysts **C1. Conditions**: pre-catalysts (0–10 μmol), DBU (4.20 mmol), CO_2 (20 bar), H_2 (40 bar), 120 °C, 24 h, THF (5 mL) and H_2O (1 mL). Products were determined by ^1H NMR and $^{13}C\{^1H\}$ NMR spectroscopy in the presence of DMF (10 μL) as an internal standard.

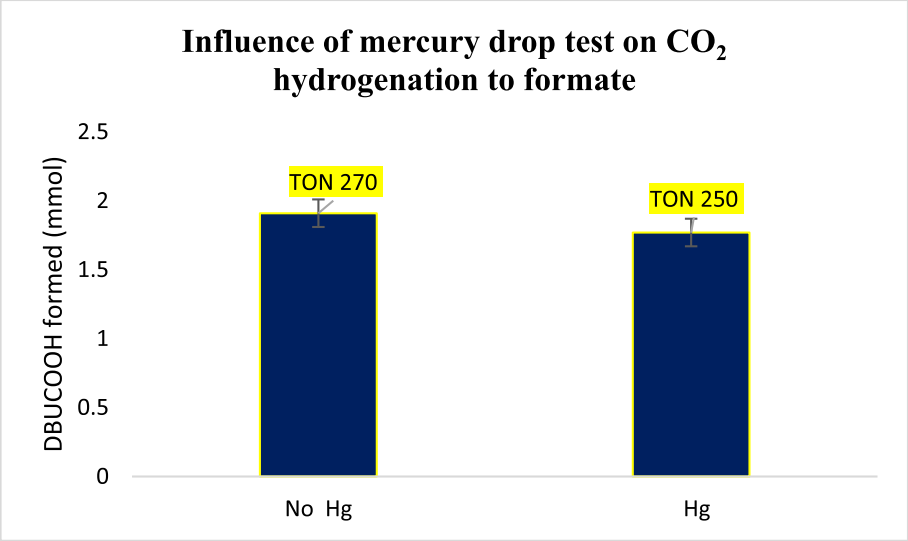

Fig. 3. Effect of mercury test on CO_2 hydrogenation with pre-catalyst **C1. Conditions**: **Conditions**: pre-catalysts (7.00 μmol), DBU (4.20 mmol), CO_2 (20 bar), H_2 (40 bar), 120 °C, elemental mercury (catalyst to mercury ratio 1:3), 24 h, THF (5 mL) and H_2O (1 mL). Products were determined by ^1H NMR and $^{13}C\{^1H\}$ NMR spectroscopy in the presence of DMF (10 μL) as an internal standard.

in conversion, with a TON of 250 compared to a similar reaction where there was no mercury added (TON of 270) (Fig. 3); a drop of only 7.5%. This suggested that catalytic activity was due to homogenous catalytic species in the system. Having established the catalyst is homogeneous, we proceeded to optimise CO_2 hydrogenation reaction with **C1**.

3.3.3. *Effect of base on hydrogenation of CO_2 with pre-catalyst **C1***

The base dependent catalytic homogenous hydrogenation of CO_2 was investigated with pre-catalyst **C1** at 120 °C in a 1:2 CO_2/H_2 mixture (60 bar) in different bases for 24 h. In the absence of a base (Table 2, entry 1) there was no product observed. This could be due to the thermodynamically unfavourable direct formic acid synthesis ($\Delta G^o_{298} = +33$ kJ mol^{-1}) [21]. It is clear from Table 2 that

Table 2
Effect of base on CO_2 with pre-catalyst **C1**.

Entry	Cat.	Base	Pressure (bar)	$HCOO^-$ (mmol)	TON	TOF (h^{-1})
1	**C1**	No base	60	0	0	0
2	**C1**	Pyridine	60	0	0	0
3	**C1**	Et_3N	60	1.5	210	8.7
4	**C1**	KOH	60	0.4	57	2.4

Conditions: base (4.20 mmol), CO_2 (20 bar), H_2 (40 bar), 120 °C, THF (5 mL), H_2O (1 mL), and 24 h. Cat. = pre-catalyst; cat loading (7 μmol). Products were determined by ^1H NMR and $^{13}C\{^1H\}$ NMR spectroscopy in the presence of DMF (10 μL) as an internal standard. Average error estimate: ±0.20 (**KOH**), ±0.19 (Et_3N). TON = (mmol of formate/mmol of pre-catalyst). TOF = TON/reaction time.

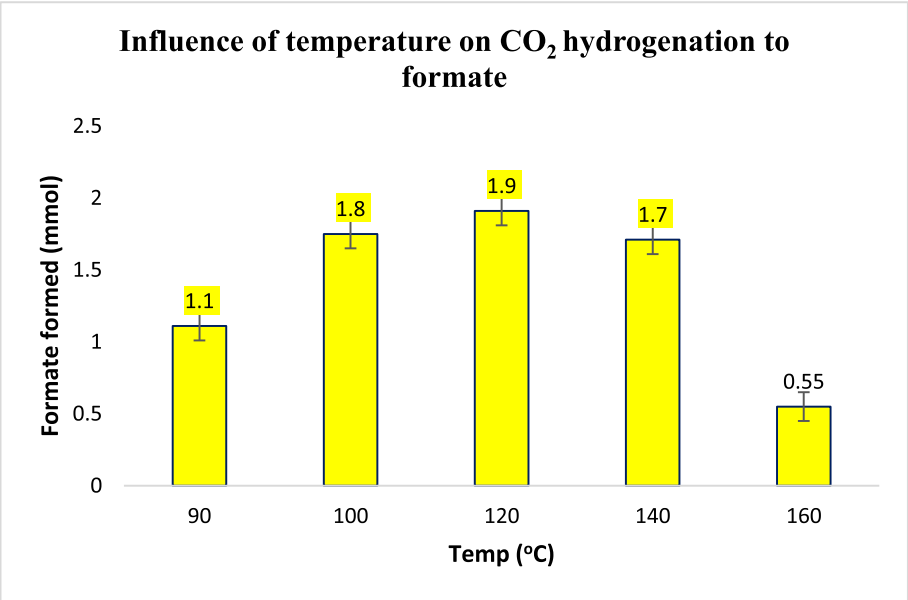

Fig. 4. Effect of temperature on CO_2 hydrogenation with pre-catalysts **C1. Conditions**: pre-catalysts (7.00 μmol), DBU (4.20 mmol), CO_2 (20 bar), H_2 (40 bar), 90–120 °C, 24 h, THF (5 mL) and H_2O (1 mL). Products were determined by ^1H NMR and $^{13}C\{^1H\}$ NMR spectroscopy in the presence of DMF (10 μL) as an internal standard.

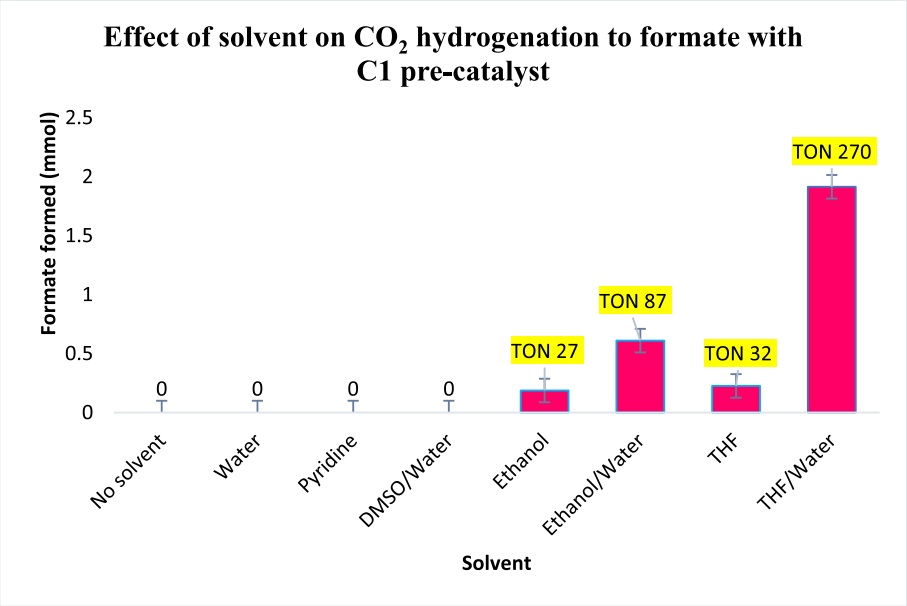

Fig. 5. Effect of solvent on CO_2 hydrogenation with pre-catalysts **C1**–C3. **Conditions**: pre-catalysts (7.00 μmol), DBU (4.20 mmol), CO_2 (20 bar), H_2 (40 bar), 120 °C, 24 h and total solvent (6 mL). Products were determined by ^{1}H NMR and $^{13}C\{^1H\}$ NMR spectroscopy in the presence of DMF (10 μL) as an internal standard.

addition of a base is necessary of the hydrogenation of CO_2 to occur; but it is the strongest DBU (that produced and the most formate (1.9 mmol). These results were expected as bases containing nitrogen have been shown to capture CO_2 during hydrogenation of CO_2 [22]. It is important to note that under acid conditions, pre-catalysts C1 could not hydrogenate CO_2. This is due to the hydrolysis of the imine bond in ligand in C1 and hence the decomposition of the catalyst.

3.3.4. *Effect of temperature on selectivity of pre-catalyst C1*

The effect of temperature on the selectivity of pre-catalyst **C1** during CO_2 hydrogenation was studied at temperatures ranging from 90 to 160 °C under standard conditions (**C1** (7.00 μmol), DBU (4.20 mmol), total pressure = 60 bar and $P(CO_2)/P(H_2)$ pressure ratio = 1:2; see Fig. 4). The catalyst could not convert CO_2 at temperatures below 90 °C, possibly due to the thermodynamic and kinetically stability of CO_2., Between 90 and 160 °C there was 100% selectivity towards formate production (Fig. 4). As the temperature increased from 90 °C to there was an increase in formate production from 1.11 mmol to 1.91 mmol. Further increase in temperature to 160 °C resulted in decrease of formate production with only 0.55 mmol of formate produced. The decrease in formate production could be caused by the pre-catalyst degrading and also due to the exothermic nature of the CO_2 hydrogenation process it is possible that there is a threshold temperature (120 °C) where any further increase in temperature is detrimental to the production of formate.

3.3.5. *Effect of solvent on the hydrogenation of CO_2 with **C1***

Solvents can play a major role in the hydrogenation of CO_2 by influencing the hydride donor ability, thus affecting the formation of active species. Changing from water to organic solvents can change the products formed during hydrogenation of CO_2 because some solvents form carbonates species and intermediates in the presence of CO_2 [23,24]. With this in mind, we investigated the effect of solvents on CO_2 hydrogenation using pre-catalysts **C1** and the conditions in Fig. 5, there was no catalytic conversion of CO_2 in the absence of a solvent. This was a clear indication that **C1** was active as a homogenous catalyst and that the reaction is solvent dependent. In water and pyridine no formate is produced due to the insolubility and partial solubility respectively of **C1** in these solvents which resulted in a hydrogenation reaction mixture which was not homogenous. It was surprising that in a DMSO/water mixture no product was observed though **C1** is completely soluble in DMSO. This could be due to the ability of DMSO coordinating to the metal centre hence competing with the substrate. In ethanol, ethanol (5 mL)/water (5 mL) and THF under our conditions there was 100% selectivity towards formate production with ethanol/water mixture and the highest TON of 87 and TOF of 3.6 h^{-1}. Ethanol is a protic solvent which could assist in the formation of hydride species which have been known to be active species in the hydrogenation of CO_2. It is the ability of the base to enhance the solubility of the complexes in ethanol and assisting in the hydrogen heterolysis to form active species that could be responsible the enhanced activity observed. But the best solvent for this reaction is THF (5 mL)/water (1 mL) mixture with a TON of 270 The biphasic nature of this reaction system made it possible for the formate to be recovered in inorganic water phase whilst the catalyst remained in the organic phase.

3.3.6. *Effect of pressure on the hydrogenation of CO_2 with **C1***

Partial pressure variation studies were performed by changing the partial pressure of CO_2 and H_2 gases but maintaining a total

Table 3
Effect of pressure on CO_2 with pre-catalyst **C1**.

Entry	Cat.	Base	$P(CO_2)/P(H_2)$ (bar/bar)	$HCOO^-$ (mmol)	TON	TOF (h^{-1})
1	**C1**	DBU	30/30	1.1	150	6.4
2	**C1**	DBU	20/40	1.9	270	11
3	**C1**	DBU	40/20	0.63	91	3.8
4	**C1**	DBU	15/45	2.2	320	13
5	**C1**	DBU	12/48	2.3	330	14

Conditions: DBU (4.20 mmol), Total pressure 60 bar, 120 °C, THF (5 mL), H_2O (1 mL), and 24 h. Cat. = pre-catalyst; cat loading (7 μmol). Products were determined by ^{1}H NMR and $^{13}C\{^1H\}$ NMR spectroscopy in the presence of 10 μL DMF as an internal standard. Average error estimate: ±0.19 (**30/30**), ±0.20 (**20/40**), ±0.17 (**40/20**), ±0.18 (**15/45**), ±0.19 (**12/48**). TON = (mmol of formate/mmol of pre-catalyst). TOF = TON/reaction time.

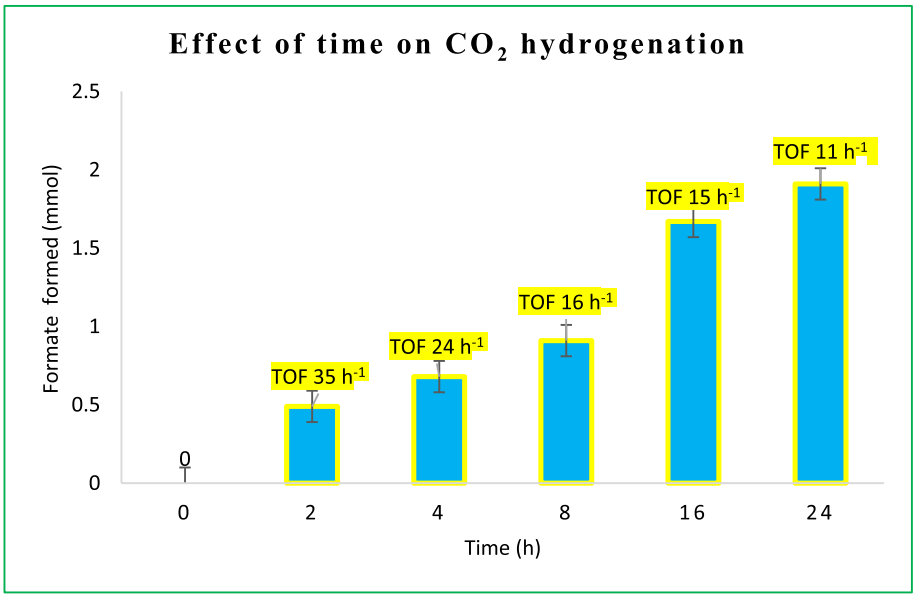

Fig. 6. Effect of time on CO_2 hydrogenation with pre-catalysts **C1. Conditions**: pre-catalysts (7.00 μmol), DBU (4.20 mmol), CO_2 (20 bar), H_2 (40 bar), 120 °C, 0–24 h, THF (5 mL) and H_2O (1 mL). Products were determined by ^1H NMR and $^{13}C\{^1H\}$ NMR spectroscopy in the presence of 10 μL DMF as an internal standard.

pressure of 60 bar (Table 3). On applying equal pressure of 30 bar CO_2 and 30 bar H_2 (Entry 1) and keeping all the other parameters constant, 1.1 mmol of formate was produced. Upon doubling the pressure of H_2 (Entry 2), the amount of formate produced almost doubled. An increase in CO_2 and decrease in H_2 (Entry 3) resulted in a decrease in formate production to 0.63 mmol. This maybe because of the effect of having only enough H_2 gas to form the hydride active species and eventually less to proceed to the hydrogenation process. An increase in H_2 pressure and decrease in CO_2 pressure resulted in an increase in formate produced. The optimum ratio for formate production is 1:4 ratio (Entry 5). Results obtained confirmed that the amount of formate produced depends on the gas pressure, but more of the partial pressure of H_2 than the partial pressure of CO_2.

3.3.7. *Reaction time effect on CO_2 hydrogenation with **C1***

Hydrogenation of $CO_2$to formate with pre-catalyst **C1** was studied at times ranging from 0 to 24 h (Fig. 6). Increasing the reaction time from 2 h to 24 h increased the amount of formate produced from 0.49 mmol to 0.91 mmol. This clearly shows the time dependent effect of the CO_2 hydrogenation to formate. The highest TOF under our reaction conditions was 35 h^{-1} after a reaction time of 2 h, but the highest amount of formate was produced in 24 h.

3.3.8. *Catalyst recyclability*

The recyclability of the active catalyst from **C1** was checked under the optimized conditions, and the results are shown in Fig. 7. The recycling tests were performed by separating the biphasic solutions *via* decantation and adding fresh substrates to the aqueous organic layer. This reaction procedure was repeated for recycling studies. The catalyst could be reused two times, maintaining a formate production of 1.9 and 1.6 mmol with 100% selectivity. The third and fourth cycle formate produced reduced to 0.35 and 0.050 mmol respectively.

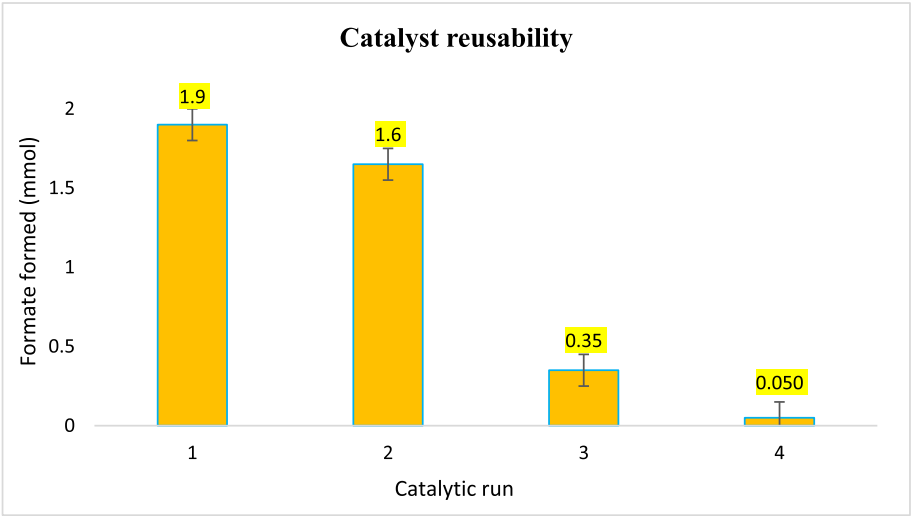

Fig. 7. Catalyst reusability on the hydrogenation of CO_2 with pre-catalyst **C1**. Conditions: pre-catalysts (7.00 μmol), DBU (4.20 mmol), CO_2 (20 bar), H_2 (40 bar), 120 °C, 24 h, THF (5 mL) and H_2O (1 mL). Products were determined by ^1H NMR and $^{13}C\{^1H\}$ NMR spectroscopy in the presence of 10 μL DMF as an internal standard.

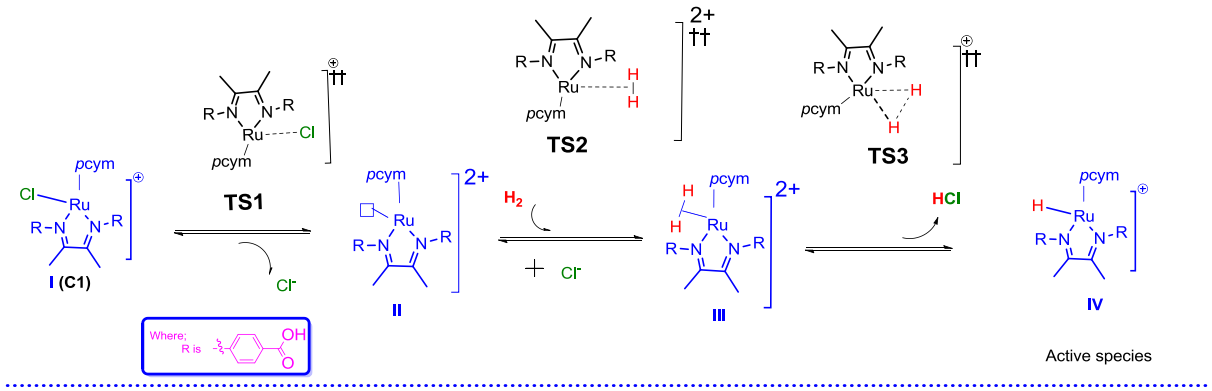

Scheme 4. Proposed reaction mechanism for the formation of Ru–H active species from complex **C1**.

3.4. *Theoretical investigation of CO_2 hydrogenation using pre-catalyst **C1***

The 100% production of formate during CO_2 hydrogenation with our novel pre-catalysts (**C1**–**C3**) inspired our goal to understand their CO_2 hydrogenation mechanism. The mechanistic studies were to investigate whether complexes **C1**–**C3** are active species or pre-catalysts in CO_2 hydrogenation reaction and to understand how CO_2 is reduced selectively to formate or methanol. In this way, it was essential to determine the thermodynamic favourability of the hydride species relative to your complex as the active species through semi-empirical or DFT calculations. This computational work aims to investigate these two aspects using novel synthesised N^N ruthenium **C1** complex which was the best performing pre-catalysts during hydrogenation of CO_2.

3.4.1. *Catalyst model: formation of the Ru–H active species*

Previously, hydrogenation of CO_2 has been proposed in various studies to involve the hydride species as the active catalyst in the reaction [25–27]. An iridium imine-diphosphine catalyst by Liu

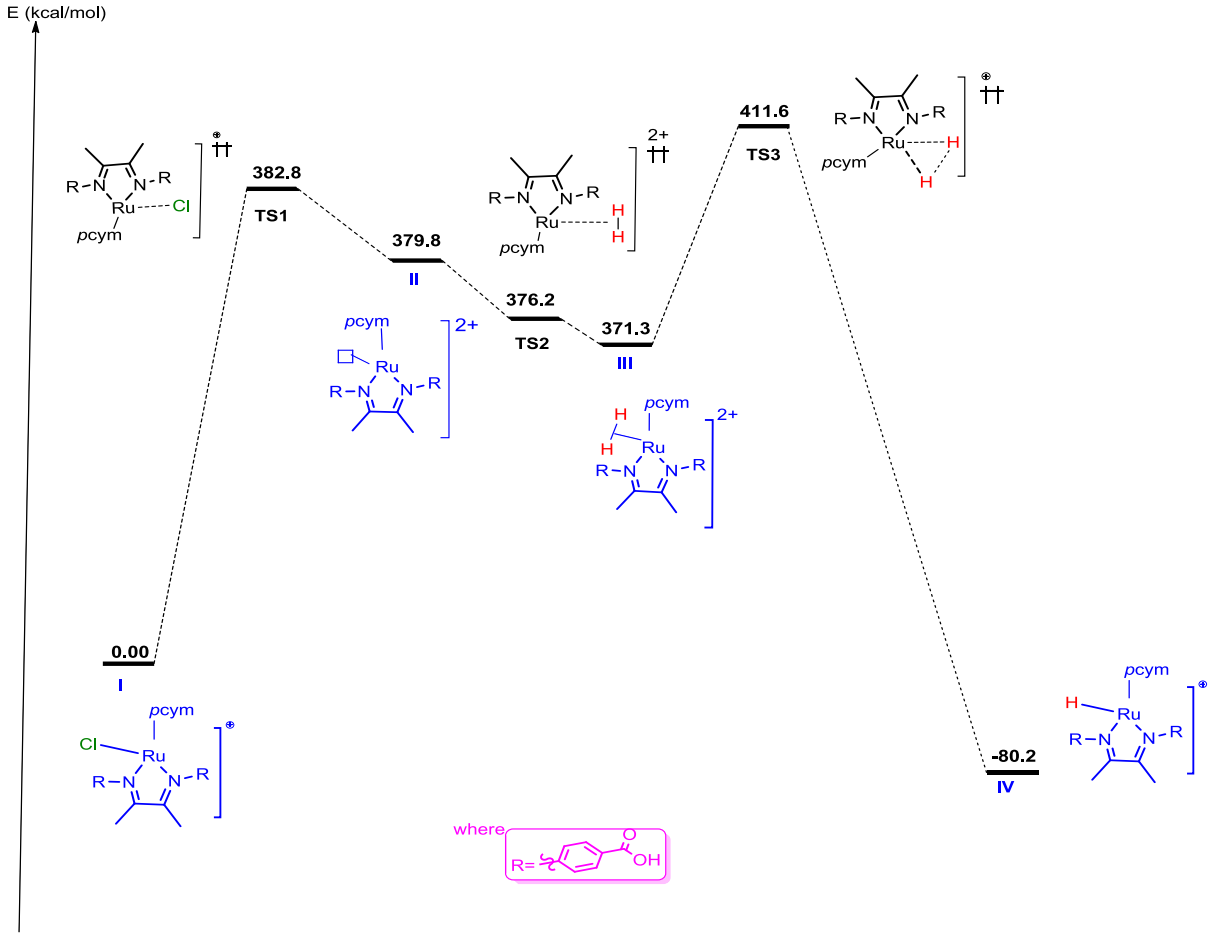

Fig. 8. DFT Energy profile for the formation of Ru–H active species.

was found to be highly active for the hydrogenation of CO_2 with the Ir–H complex being the active species and a TON value of 450 000 was achieved [28]. Comparative analysis of these literature reports with our experimental design enabled us to focus on formation of ruthenium hydride species as our initial step in computational studies through DFT calculations.

We rationalized three steps to our proposed ruthenium hydride (Scheme 4) as the active species, these include *(i)* reductive elimination *(ii)* 16-electron cationic complex (solvate) formation *(iii)* hydrogen insertion. The first step is reductive elimination of the chloride from the cationic ruthenium (II)-chloride complex **C1** to form a cationic complex **II. II** was formed through conversion of the 18-electron complex **I** to a 16-electron complex with a vacant site for the coordination of the H_2 molecule.

Intermediate **III**, a dihydrogen complex, is formed through insertion of H_2 *via* **TS2** which is enabled by the δ-donation the H_2 and the π–backdonation of the Ru metal centre. The active species **IV** is formed after elongation of the dihydrogen complex **TS3** with hydrogen splitting with elimination of HCl. The proposed mechanism was studied with DFT/MO6 to give an energy profile Fig. 8. According to Fig. 8, the elimination of Cl^- (through transition state **TS1**) is the first rate-determining step with an activation energy of 382.8 kcal/mol followed by the second-rate determining step through **TS3** with an energy of 411.6 kcal/mol relative to the starting material **I**. It is important to note that the active species with an energy of −80.2 kcal/mol is the most stable species of in this cycle.

3.4.2. *Formate formation from CO_2 hydrogenation*

The hydrogenation of CO_2 with N^N Ru pre-catalyst (Scheme 4, **structure I**) at 120 °C with a pressure of 60 bars (1 CO_2:2H_2) resulted in formation of formate in the presence of a base. These findings led us to the investigations of the mechanism associated with formate formation with our pre-catalyst. The computational studies for the mechanism for formate formation (Scheme 5), were carried out under vacuum. The catalytic cycle proceeds from the pre-catalyst I which proceeds to the formation of the active species, the Ru–H complex (**IV**) according to Scheme 4.

The insertion of CO_2 *via* associative addition generates the formate complex (**V**) which readily dissociates the formate to regenerate the 16-electron complex (**II**). Complex **V** was not observed with ^{1}H NMR but the formate product was observed in the presence of a base. This could be due to the rapid exchange of the complex formate (**V**) with hydronium ion H_3O^+ to produce HCOOH in the presence of solvent [29]. This was also observed

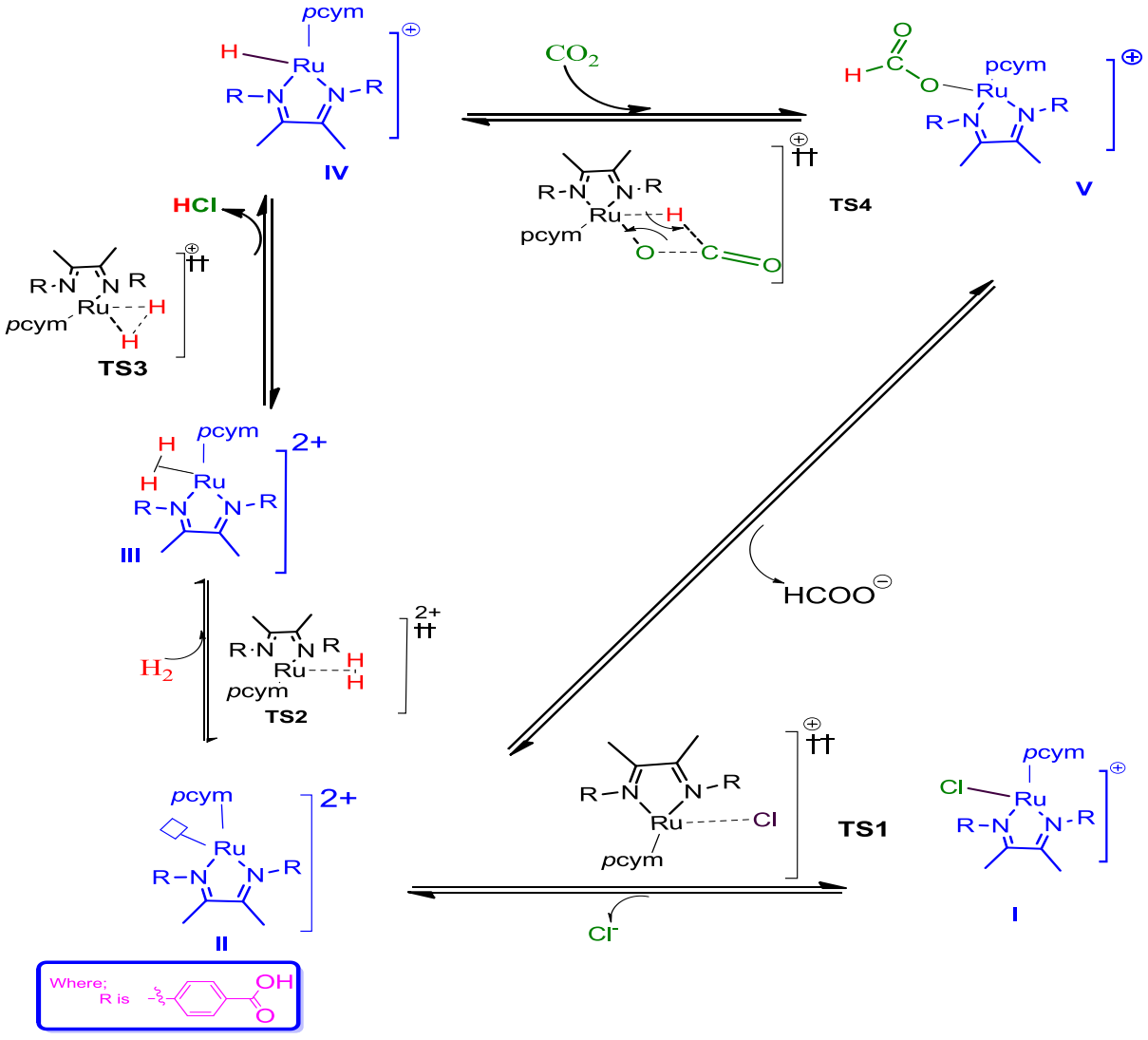

Scheme 5. Proposed mechanism for hydrogenation of CO_2 to formic acid.

through DFT calculations by Osadchuk and co-workers involving the sequential insertion of two CO_2 molecules in two Ir−H bonds before hydrogenation [30]. From Fig. 9, transition state **TS4** which is the insertion of CO_2 requires an energy of 142.1 kcal/mol relative to intermediate I after formation of **IV**. After the formation of the Ru−H active species, Fig. 9 shows that CO_2 insertion is the rate determining step with the highest energy barrier which could be due to the thermodynamic stability of CO_2.

3.4.3. *Methanol formation from CO_2 hydrogenation*

The insertion of CO_2 into a metal hydride bonds and successive formation of metal-formate complexes has been studied both experimentally and theoretically by various researchers [31–34]. The mechanistic studies of CO_2 hydrogenation to methanol has been extensively studied theoretically and supports that the hydrogenation to methanol include HCOO*, HCOOH*, CH_3O_2* and CH_3O* intermediates [35–39]. Based on literature and evidence from our ^1H and $^{13}C\{^1H\}$ NMR experiments [38,40], a plausible catalytic cycle that reduces CO_2 to methanol step wisely through formic acid (and formaldehyde theoretically) *via* key intermediates **I**, **III**, **IV**, **V** and **VI** was developed as proposed in Scheme 6.

Scheme 6 show that the cycle starts from cationic Ru−H complex **I** with (migratory) insertion of CO_2 to ruthenium hydride species **I** which leads to a Ru-formate species **III**. Reaction of **IV** with one equivalent of hydrogen leads to the formation of Ru-hydromethanolate species, **V** which upon further reduction formic acid transforms to Ru-methanolate complex **VI**. Hydrogenolysis of Ru−OMe complex requires a third equivalent of hydrogen to liberate the product and closing of the cycle to regenerate Ru−H complex **I**.

The first step in the mechanism of the formation of methanol from CO_2 hydrogenation (Fig. 10), is the insertion of CO_2 into the Ru−H bond forming a Ru−O bond *via* **TS4** with an energy of 114.7 kcal. Intermediate **III** (70.1 kcal/mol) is more stable than intermediate **IV** (78.6 kcal/mol). Similar results have been reported by Wesselbaum and co-workers who carried out mechanistic investigations of multiphase catalysis for CO_2 hydrogenation to methanol with a homogenous ruthenium-Triphos catalyst [38]. The insertion of H_2 *via* **TS6** from intermediate **IV** is considered as the rate determining step with an energy of 160.2 kcal/mol relative to the intermediate **I**. However, **TS5** and **TS7** could not be located and this could be due to different modes of H_2 coordination to the Ru metal centre or due to a missing intermediate in the proposed cycle but they have been reported by exist by Wesselbaum and co-workers [38]. The energy profile proceeds to the methoxy intermediate, **VI** (121.7 kcal/mol) followed by the liberation of methanol *via* **TS8** (140.1 kcal/mol) then regeneration of the active species **I** (−80.2 kcal/mol) which is relatively more stable than all the intermediates.

4. Conclusion

The main thrust of the work is to synthesise imine-based complexes containing carboxylic acid moieties for the hydrogenation of CO_2 to formate. Metalation of L with $[RuCl_2$ (p-cymene)$]_2$, $[Ir(\eta^5\text{-}C_5Me_5)Cl_2]_2$ and $[Rh(\eta^5\text{-}C_5Me_5)Cl_2]_2$ afforded novel PGM complexes **C1**, **C2 and C3** which were tested as pre-catalysts for the hydrogenation of CO_2. Hydrogenation of CO_2 to formate with H_2 gas was achieved under moderate conditions with the highest TON and

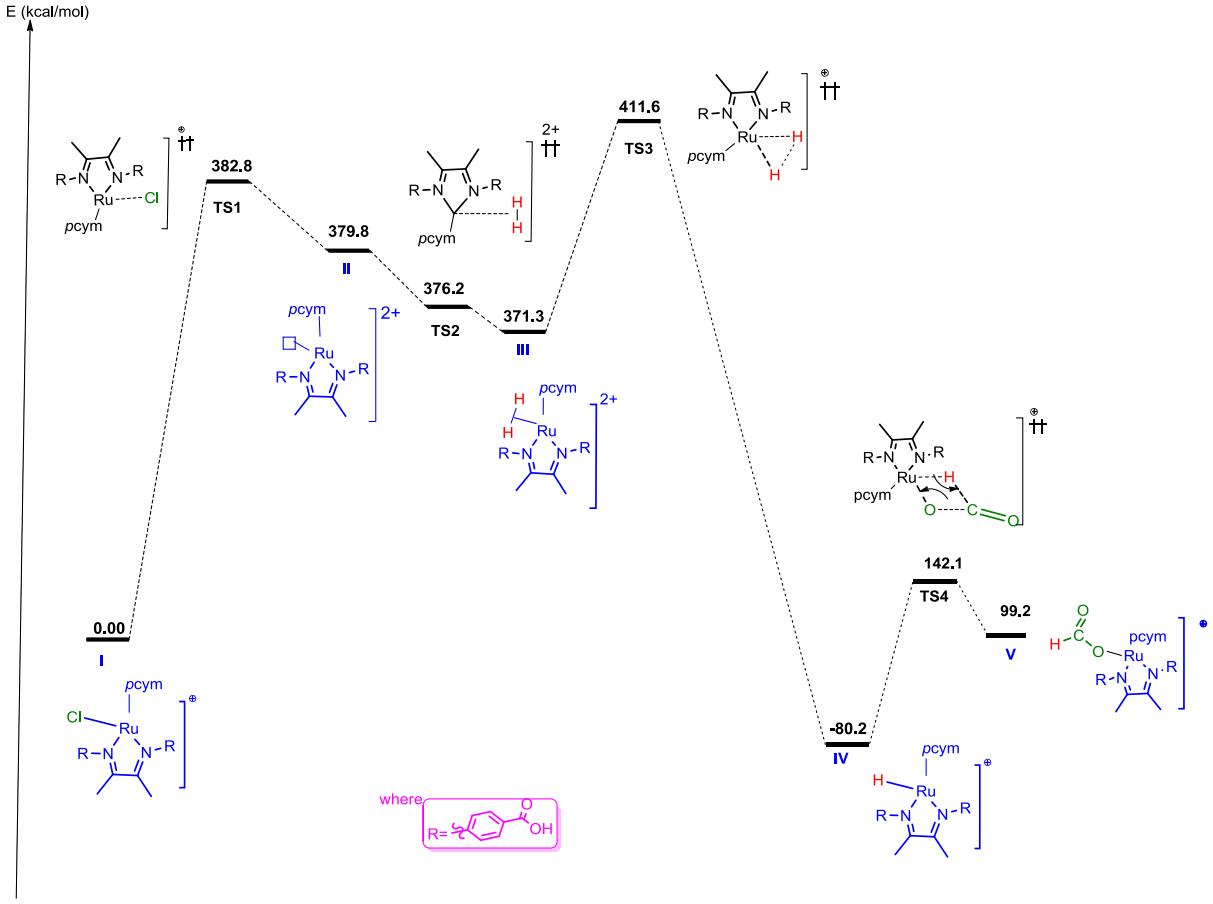

Fig. 9. Energy profile for the hydrogenation of CO_2 to formate.

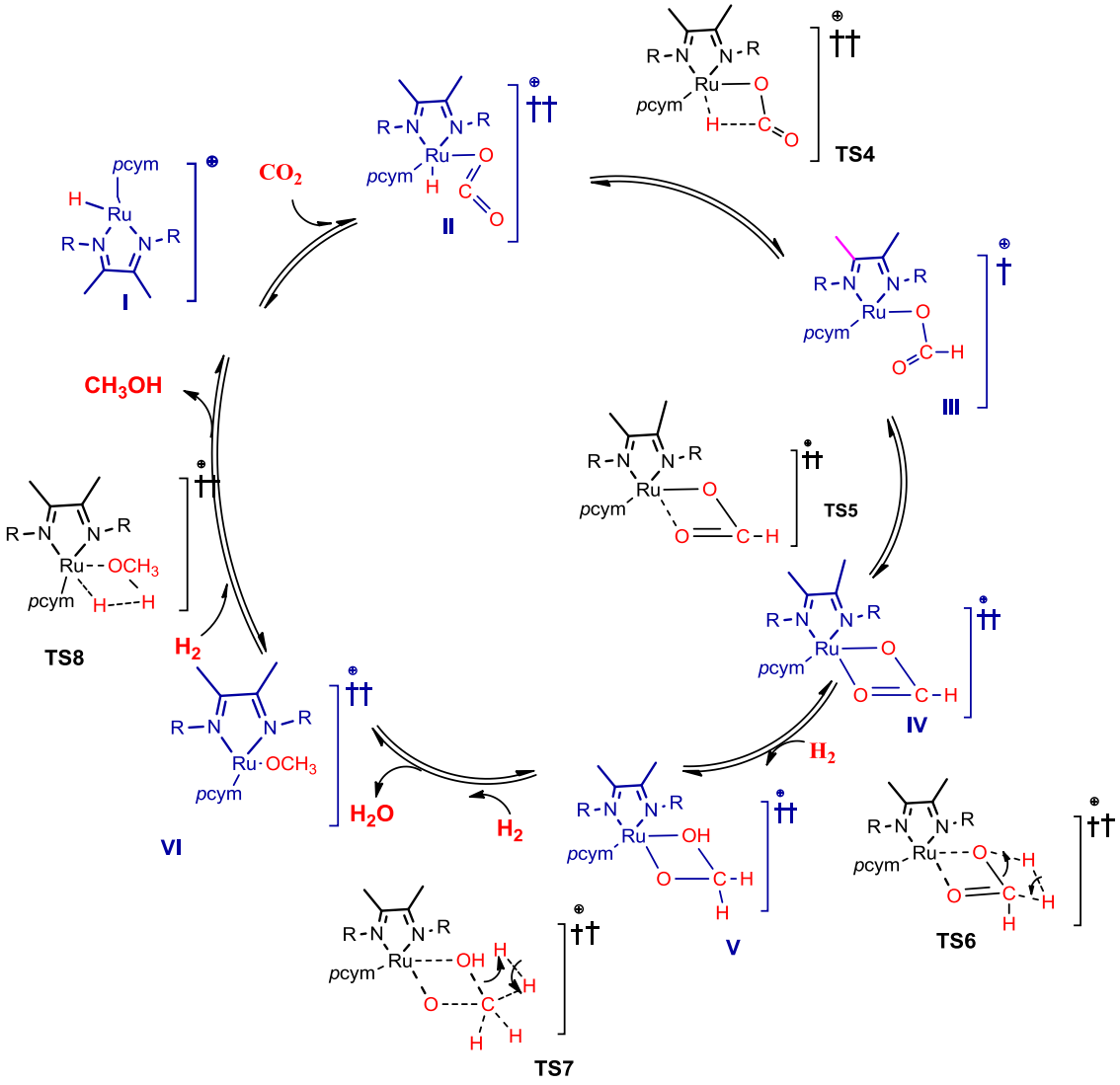

Scheme 6. Proposed catalytic mechanism for hydrogenation of CO_2 to methanol in the absence of a base.

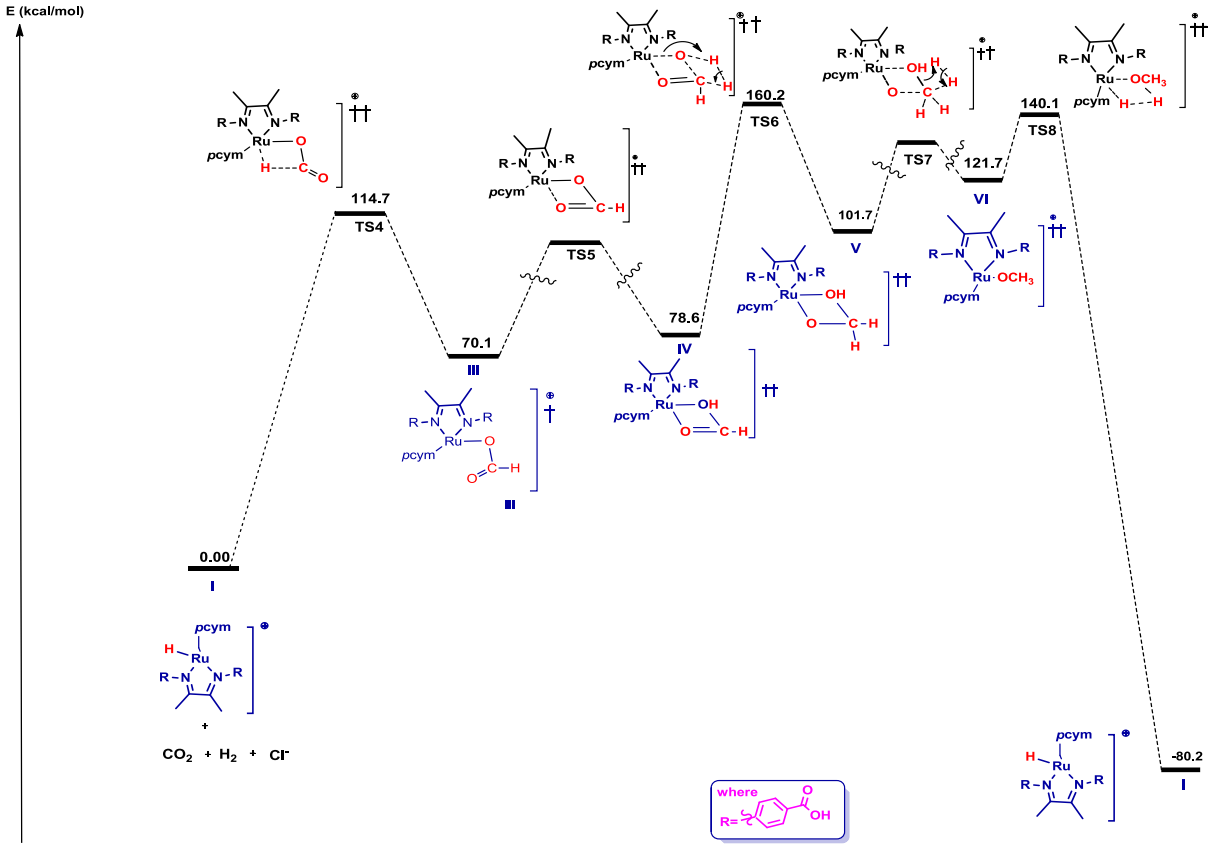

Fig. 10. Energy profile for the hydrogenation of CO_2 to methanol.

TOF of 320 and 35 h^{-1} respectively at 120 °C with **C1**. Remarkably, the biphasic nature of the hydrogenation process brings about easy catalysts recovery and recycling. This work is important as it has demonstrated new imine-based Ru^{II}, Ir^{III} and Rh^{III} complexes as pre-catalyst for the one-step synthesis of formate from CO_2 hydrogenation whilst addressing CO_2 conversion issues. In the future, we expect to modify the properties of L with electron withdrawing and donating groups to obtain better TON and TOF values under lower temperature and pressure reaction conditions. The mechanistic studies for the hydrogenation of **C1**–**C3** as pre-catalysts in the formation of formate and methanol was studied using **C1** with density functional theory calculation. Theoretical mechanistic studies for complex **C1** calculated using DFT/MO6 show that the active species is ruthenium hydride hence the synthesised complexes act as pre-catalysts. The high energy values associated with the formation of methanol explains why we could not obtain methanol under our reaction conditions. These studies are significant in designing and elucidating new catalytic active catalysts/species for the hydrogenation of CO_2.

Acknowledgements

Financial support by South Africa's National Research Fund (NRF) in partnership with The World Academy of Sciences (TWAS) (Grant Numbers: 99978 and 117989), The Technology and Human Resource for Industry Programme (THRIP), (Grant Number: THRIP/58/30/11/2017), Sasol SA Ltd (University Collaboration Programme) is greatly appreciated. The authors are also grateful to the University of Johannesburg's Division of Internationalization (Study Abroad Programme) and the UJ Centre for Synthesis & Catalysis for funding.

Appendix A. Supplementary data

Supplementary data to this article can be found online at https://doi.org/10.1016/j.jorganchem.2019.120892.

References

[1] C. Hou, J. Jiang, S. Zhang, G. Wang, Z. Zhang, Z. Ke, C. Zhao, ACS Catal. 4 (2014) 2990–2997.
[2] A. Dubey, L. Nencini, R.R. Fayzullin, C. Nervi, J.R. Khusnutdinova, ACS Catal. 7 (2017) 3864–3868.
[3] A. Behr, K. Nowakowski, Catalytic Hydrogenation of Carbon Dioxide to Formic Acid, vol. 66, 2014.
[4] R. Kanega, N. Onishi, D.J. Szalda, M.Z. Ertem, J.T. Muckerman, E. Fujita, Y. Himeda, ACS Catal. 7 (2017) 6426–6429.
[5] Y. Himeda, Eur. J. Inorg. Chem. (2007) 3927–3941.
[6] N.N. Ezhova, N.V. Kolesnichenko, A.V. Bulygin, E.V. Slivinskii, S. Han, Russ. Chem. Bull. Int. Ed. Izv. Akad. Nauk. Seriya Khimicheskaya 51 (2002) 2165–2169.
[7] P. Munshi, A.D. Main, J.C. Linehan, C.C. Tai, P.G. Jessop, J. Am. Chem. Soc. 124 (2002) 7963–7971.
[8] Y. Maenaka, T. Suenobu, S. Fukuzumi, Energy Environ. Sci. 5 (2012) 7360–7367.
[9] E. Carmona, A. Cingolani, F. Marchetti, C. Pettinari, R. Pettinari, B.W. Skelton, A.H. White, Organometallics 22 (2003) 2820–2826.
[10] Y. Hu, L. Li, A.P. Shaw, J.R. Norton, W. Sattler, Y. Rong, Organometallics 31 (2012) 5058–5064.
[11] Y. Yang, W. Zhang, X. Ma, H. Zhao, X. Zhang, ChemCatChem 102249 (2015) 3454–3459.
[12] B.P. Buffin, A. Kundu, Inorg. Chem. Commun. 6 (2003) 680–684.
[13] X.Y. Liu, K.S. Lokare, S.K. Ganesh, J.M. Gonzales, J. Oxgaard, W. Goddard, R. Periana, Dalton Trans. 40 (2011) 301–304.
[14] S.J. Lucas, R.M. Lord, R.L. Wilson, R.M. Phillips, V. Sridharan, P.C. McGowan, Dalton Trans. 41 (2012) 13800–13802.
[15] A.L. Spek, Acta Crystallogr. Sect. D Biol. Crystallogr. 65 (2009) 148–155.
[16] A.L. Spek, J. Appl. Crystallogr. 36 (2003) 7–13.
[17] S. Ogo, R. Kabe, H. Hayashi, S. Fukuzumi, Dalton Trans. (2006) 4657–4663.
[18] E. F, Y.H. Wan-Hui Wang, Jonathan F. Hull, James T. Muckerman, Energy

Environ. Sci. (2012) 7923–7926.
[19] R. Tanaka, M. Yamashita, L.W. Chung, K. Morokuma, K. Nozaki, Organometallics 30 (2011) 6742–6750.
[20] M.L. Man, Z. Zhou, S.M. Ng, C.P. Lau, Dalton Trans. 2 (2003) 3727–3735.
[21] R. Van Putten, T. Wissink, T. Swinkels, E.A. Pidko, Int. J. Hydrogen Energy 1–9 (2019).
[22] P. Patel, S. Nandi, M.S. Maru, R.I. Kureshy, N.H. Khan, J. CO2 Util. 25 (2018) 310–314.
[23] G. Jacobs, B.H. Davis, Catalysis 20 (2007) 122–285.
[24] S.A. Burgess, A.M. Appel, J.C. Linehan, E.S. Wiedner, Angew. Chem. Int. Ed. 560 (2017) 15002–15005.
[25] W. Wang, S. Wang, X. Ma, J. Gong, Chem. Soc. Rev. 40 (2011) 3703–3727.
[26] Y.-N. Li, R. Ma, L.-N. He, Z.-F. Diao, Catal. Sci. Technol. 4 (2014) 1498–1512.
[27] F. Bertini, N. Gorgas, B. Stöger, M. Peruzzini, L.F. Veiros, K. Kirchner, L. Gonsalvi, ACS Catal. 6 (2016) 2889–2893.
[28] C. Liu, J.-H. Xie, G.-L. Tian, W. Li, Q.-L. Zhou, Chem. Sci. 6 (2015) 2928–2931.
[29] T. Koike, T. Ikariya, Adv. Synth. Catal. 346 (2004) 37–41.
[30] I. Osadchuk, T. Tamm, M.S.G. Ahlquist, Organometallics 34 (2015) 4932–4940.
[31] M. K. Whittlesey, R. N. Perutz and M. H. Moore, 1996, 2, 5166–5169.
[32] P. Anderson, G.B. Deacon, K.H. Haarmann, F.R. Keene, T.J. Meyer, D. Reitsma, B.W. Skelton, G.F. Strouse, N.C. Thomas, J. Treadway, A.H. Whit, Inorg. Chem. 34 (1995) 6145–6157.
[33] H. S. Chu, C. P. Lau, K. Y. Wong and W. T. Wong, 1998, 7333, 2768–2777.
[34] Y.Y. Ohnishi, Y. Nakao, H. Sato, S. Sakaki, Organometallics 25 (2006) 3352–3363.
[35] Z.M. Hu, K. Takahashi, H. Nakatsuji, Surf. Sci. 442 (1999) 90–106.
[36] L.C. Grabow, M. Mavrikakis, ACS Catal. 1 (2011) 365–384.
[37] A.A. Peterson, F. Abild-Pedersen, F. Studt, J. Rossmeisl, J.K. Nørskov, Energy Environ. Sci. 3 (2010) 1311.
[38] S. Wesselbaum, V. Moha, M. Meuresch, S. Brosinski, K.M. Thenert, J. Kothe, T. Vom Stein, U. Englert, M. Hölscher, J. Klankermayer, W. Leitner, Chem. Sci. 6 (2015) 693–704.
[39] X. Yang, ACS Catal. 1 (2011) 849–854.
[40] S. Wesselbaum, T. Stein, J. Klankermayer, W. Leitner, Carbon N. Y. 3 (2012) 1–5.